Alireza Ramezani
Department of Mechanical Engineering,
University of Michigan,
Ann Arbor, MI 48109
e-mail: aramez@umich.edu

Jonathan W. Hurst
Professor
Department of Mechanical Engineering,
Oregon State University,
Corvallis, OR 97331
e-mail: jonathan.hurst@oregonstate.edu

Kaveh Akbari Hamed
Department of Electrical Engineering,
University of Michigan,
Ann Arbor, MI 48109
e-mail: kavehah@umich.edu

J. W. Grizzle
Professor
Department of Electrical Engineering,
University of Michigan,
Ann Arbor, MI 48109
e-mail: grizzle@umich.edu

Performance Analysis and Feedback Control of ATRIAS, A Three-Dimensional Bipedal Robot

*This paper develops feedback controllers for walking in 3D, on level ground, with energy efficiency as the performance objective. **A**ssume **T**he **R**obot **I**s **A** **S**phere (ATRIAS) 2.1 is a new robot that has been designed for the study of 3D bipedal locomotion, with the aim of combining energy efficiency, speed, and robustness with respect to natural terrain variations in a single platform. The robot is highly underactuated, having 6 actuators and, in single support, 13 degrees of freedom. Its sagittal plane dynamics are designed to embody the spring loaded inverted pendulum (SLIP), which has been shown to provide a dynamic model of the body center of mass during steady running gaits of a wide diversity of terrestrial animals. A detailed dynamic model is used to optimize walking gaits with respect to the cost of mechanical transport (CMT), a dimensionless measure of energetic efficiency, for walking speeds ranging from 0.5 (m/s) to 1.4 (m/s). A feedback controller is designed that stabilizes the 3D walking gaits, despite the high degree of underactuation of the robot. The 3D results are illustrated in simulation. In experiments on a planarized (2D) version of the robot, the controller yielded stable walking.*
[DOI: 10.1115/1.4025693]

1 Introduction

This paper develops feedback controllers for walking in 3D, on level ground, with energy efficiency as the performance objective for an underactuated bipedal robot. The 3D bipedal robot [1] ATRIAS 2.1 shown in Fig. 1 represents a collaborative effort of Oregon State University, Carnegie Mellon University, and the University of Michigan. The robot has been conceived for energy efficiency, speed, and robustness with respect to natural terrain variations, without over-reliance on external sensing, such as vision. The robot is untethered, with all computation and power on board, using electric motors, batteries, and mechanical springs for cyclic gait-energy storage.

The legs of ATRIAS 2.1 are very light (less than 5% of total mass) and are driven by series-elastic actuators. The torso accounts for approximately 40% of the mass of the robot, with its center of mass approximately 30 cm above the hip. The series-elastic actuators in the legs are powered by electric motors through a 50:1 harmonic drive. Hence, the reflected inertia of the rotors of the motors dominate leg rotation, while the light legs and springs dominate the impact dynamics. The robot has 6 actuators and in single support has 13 degrees of freedom (DOF).

The paper is organized as follows. Section 2 describes the design philosophy of ATRIAS 2.1 and an overview of the mechanism. Similarities and differences of ATRIAS 2.1 with respect to existing robots are discussed in Sec. 3. A dynamic model appropriate for walking gaits is given in Sec. 4. Section 5 overviews the hybrid zero dynamics (HZD) as a gait optimization and design tool. This section also addresses the selection of virtual constraints adapted to the morphology of the robot. Section 6 introduces a family of functions, nonuniform rational basis spline (NURB), to parameterize the virtual constraints. Some advantages of NURBS over Bézier polynomials for gait design are highlighted. Section 7 analyzes the walking efficiency of the 3D model of ATRIAS 2.1 measured by the CMT [2], for average walking speeds varying from 0.5 to 1.4 (m/s). The evolution of important physical quantities such as positive work, negative work, ground reaction force, are highlighted. Section 8 presents a continuous-time time-invariant feedback controller based on virtual constraints and input–output linearization to asymptotically stabilize one of the walking gaits obtained using the HZD optimization. Stability is checked with a Poincaré section analysis. The continuous-time feedback

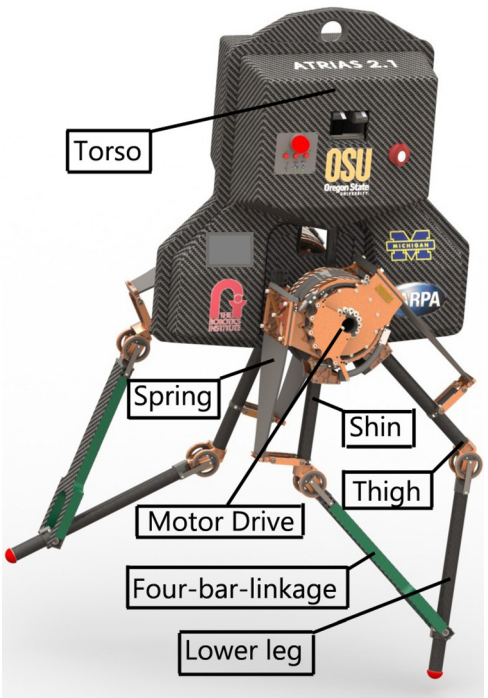

Fig. 1 Untethered 3D bipedal robot ATRIAS 2.1

Contributed by the Dynamic Systems Division of ASME for publication in the Journal of Dynamic Systems, Measurement, and Control. Manuscript received December 3, 2012; final manuscript received October 7, 2013; published online December 9, 2013. Assoc. Editor: Luis Alvarez.

controller is augmented with an event-based controller to stabilize gaits in the 3D model. Finally, Sec. 9 presents concluding remarks.

The feedback designs of Sec. 8 have been implemented on a planarized version of the robot, where lateral stability is assured by a boom, as shown in the video [3]. Stable walking was achieved three days after the robot was assembled. While this initial success was quite welcome, it could still take a year to implement the feedback policies developed herein for the 3D case.

2 Testbed Overview

2.1 Design Philosophy. ATRIAS 2.1 is a 3D bipedal robot as shown in Fig. 1. The name is an acronym which stands for **A**ssume **T**he **R**obot **I**s **A** **S**phere; a reference to the design goal of creating a mechanical system that is dynamically simple and easy to model and control. The robot's sagittal plane dynamics are designed to embody the SLIP model, which has been shown to approximate the body center-of-mass motion during *steady-state running gaits* of a wide diversity of terrestrial animals, [4–8]. Successful running robots, such as the Planar Hopper, ARL Mono pod II, and CMU Bowleg Hopper, also exhibit SLIP model behavior [9–11]. An earlier machine by Hurst and Grizzle, the planar bipedal robot MABEL, also approximates a SLIP model; the robot achieved a peak walking speed of $1.5(\mathrm{m/s})$ [12]; a peak running speed of $3(\mathrm{m/s})$ [13]; and walked over terrain with variations exceeding 15% of leg length [14,15].

These robots demonstrate that spring-mass models are a successful and promising approach to machine design for robotic running. It is also promising for walking gaits—the same spring-mass model arranged in a bipedal pair has also been shown, in simulation, to reproduce steady-state dynamics of human walking [16]. ATRIAS 2.1 takes the spring-mass design philosophy into 3D, and combines it with tether-free electric actuation.

2.2 Mechanism. ATRIAS is constructed of a pair of identical legs, each with two DOF, mounted to a torso by a frontal plane revolute joint, for a total of six actuated DOF. Each leg is comprised of a pair of powerful brushless motors located at the hip joint, each connected through a 50:1 harmonic drive and a large spring to a 4-bar linkage, as shown in Fig. 2(*a*). The motors each actuate one link of the 4-bar linkage through a series spring with stiffness chosen to coincide with the natural frequency of the preferred locomotion gait, and sized large enough to store gait energy. The 4-bar linkage allows the leg to be extremely lightweight, which minimizes the impact losses of the foot during touchdown of each stride, and maximizes the gait energy that can be stored in the springs and recycled.

The torso houses the on board real-time computing, batteries, and motors for actuating the frontal plane motion of the legs, and hence accounts for approximately 40% of the mass of the robot. For the purposes of control, we have assigned axes x-y-z to the torso, oriented so that the z-axis points upward and the y-axis points forward. The left and right hip are connected to the torso through revolute joints with a common axis aligned with the y-axis of the torso. Each hip is independently actuated in the frontal plane by a brushless DC-motor connected through a gear ratio of 26.7:1. As indicated above, these motors are mounted on the torso.

Each hip is approximately 15 cm wide, so that the total width of the hips when they are parallel is 30 cm. At the current time, the legs are terminated in point feet for simplicity. Nontrivial feet may be added later, to explore potential improvements in efficiency and robustness.

It follows that the robot is highly underactuated. Indeed, when ATRIAS 2.1 is not in contact with the environment, it has sixteen DOF and six independent actuators. Six DOF are associated with the translation and orientation of the torso. There are two DOF where the hips attach to the torso, and each leg has four DOF with two DOF arising from the 4-bar mechanism and an additional two DOF due to the springs.

2.3 Nominal Parameters. Our team is maintaining a web site to document the modeling parameters for ATRIAS 2.1 [17]. *SolidWorks* has been used to compute the COM and inertia tensor of the components of the robot. Parameters for the springs, motor inertia, motor gear ratio, and harmonic drive are reported by the manufacturer. Later, these will be verified by system/parameter identification.

3 Relation to Other Robots

A number of robots have been built for the purposes of walking and running, [18–21]. One class of robots relies on large actuators and active control to implement a variety of behaviors. Examples include robots with rigid transmissions such as Rabbit and Asimo [20,21]. While these robots are capable of an aerial phase, it is at the expense of heavy actuators with high energetic cost and potentially unpredictable dynamic behavior at ground impact. At the other end of the spectrum, the McGeer walker and similar robots use only passive elements. These robots can efficiently walk down

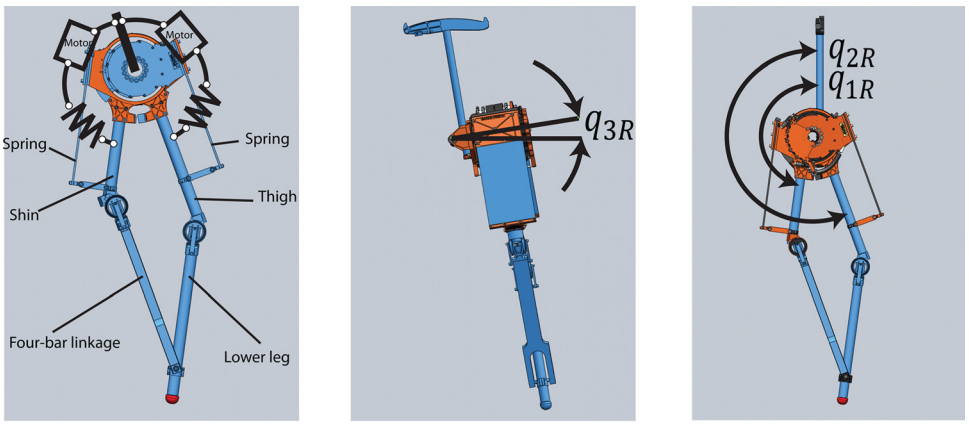

(a) (b) (c)

Fig. 2 The right leg of the robot. (*a*) The 4-bar parallelogram that forms each leg and a conceptual representation of the series-elastic actuators. (*b*) The configuration variable q_{3R} is the rotation of the right hip in the frontal plane; q_{3L} is similar. (*c*) q_{1R} and q_{2R} are the angles between the right upper links and the torso; q_{1L} and q_{2L} are defined similarly.

shallow slopes, but are extremely sensitive to disturbances and hard code only a single behavior [22,23].

There are robots that fall in between those two extremes. For instance, the "Cornell Ranger" adds minimal actuation at the ankle to its reliance on passive dynamics, and can maintain a very efficient walking gait on flat ground. Yet this and similar machines [2,24] retain the extreme sensitivity of passive dynamic walkers to disturbances and the focus on only one dynamic behavior.

The MIT Leg Lab's "Spring Flamingo" walking biped and Boston Dynamics' "BigDog" walking and running quadruped both use series springs, a passive dynamic element, to improve the performance of their actuators in certain situations. Like the rigid-transmission robots, however, they attempt to create all gait dynamics through software control [25,26]; the springs on these robots are primarily for force sensing and mechanical filtering purposes, and are essentially a soft load cell, acting as a force sensor for the low-level controllers [27]. Although this approach can result in impressive agility and robustness surpassing a rigid system, the energetic cost is still very high. For example, Big Dog uses a gasoline engine as a power source. Very recently, robots are being purposely built with high-bandwidth actuators and no springs with the objective of implementing compliance in software. Examples include the hydraulically-actuated HyQ [28] and MIT's electrically-powered Cheetah [29].

The jury is still out on which design philosophy will provide the best tradeoffs in terms of agility, efficiency, and ease of control. ATRIAS 2.1 is very much in the camp of seeking to combine the advantages of passive dynamics with actuation and feedback control for achieving a wide range of legged mobility. Its design exploits springs for energy-efficient steady-state locomotion and accommodating large disturbances, while using powerful actuators to achieve legged dexterity and gait stability when needed during transient behaviors.

4 Dynamic Model of Walking

4.1 Generalized Coordinates. Coordinates are defined for the robot in general position, that is, when neither leg is in contact with the ground. When the robot is in single support, meaning one and only one leg is in contact with the ground, appropriate holonomic constraints can be applied to arrive at a reduced set of generalized coordinates. The coordinates are defined independent of which leg is eventually the stance leg; this is different from the approach followed in Ref. [30]. All relative angles are positive in the direction that respects the right-hand rule with one exception, the left hip joint angle.

Let a world frame be defined and attach a Cartesian coordinate frame (x_T, y_T, z_T) to the torso, oriented so that when the torso is upright, the z-axis points upward and the y-axis points forward. Euler angles are used to parameterize the orientation of the torso with respect to the world frame. These angles are denoted by q_z, q_x, and q_y and are called yaw, pitch, and roll, respectively. The yaw coordinate of the torso is also called heading. The angles of the right and left hips relative to the torso are denoted by q_{3R} and q_{3L}, respectively, as shown in Fig. 2(*b*). Because the four links in each leg form a parallelogram, only two coordinates are needed to parameterize the four links. The angles of the top two links relative to the hip are denoted by q_{1R} and q_{2R} for the right leg, and q_{1L} and q_{2L} for the left leg. This completes the coordinates for the body of the robot; see Fig. 2(*c*).

Turning to the actuators, because the motors at the hips are connected to the body through a fixed gear ratio, the angles of the rotors relative to the torso are uniquely determined from q_{3R} and q_{3L}. On the other hand, the motors driving the legs are connected through springs, and hence additional coordinates are needed. For each motor, the angle of the output shaft of the harmonic drive is denoted by q_{gr}. These angles are used instead of the angles of the rotors of the motors because q_{gr1R}, q_{gr2R}, q_{gr1L}, and q_{gr2L} are in the "same coordinate frame" as the link angles of the legs.

4.2 Single-Support 3D Dynamic Model. When in single support, the Cartesian coordinates of the torso are redundant and can be eliminated. Hence, for developing the single-support model, with either the left or the right leg in stance, the configuration variables are $q_s = (q_z, q_y, q_x, q_{1R}, q_{2R}, q_{1L}, q_{2L}, q_{gr1R}, q_{gr2R}, q_{3R}, q_{gr1L}, q_{gr2L}, q_{3L})$. We note that the last 6 coordinates are independently actuated, whereas the first 7 coordinates are unactuated. Let $Q_s \subset SO(3) \times \mathbb{S}^{10}$ be a connected open subset giving the feasible set for the configuration variables.

The model and its feasible set of variables will of course depend on which leg is in stance. This will be made clear in Sec. 4.4 by appending a subscript "L" or "R" as appropriate.

Because the 4-bar linkage in each leg forms a parallelogram, the linear and angular velocities of the lower two links are identical to the linear and angular velocities of the corresponding upper links. It follows that the Lagrangian of the model can be developed as if the robot were a pinned open kinematic chain [31, p. 408]. To compute the Lagrangian, the kinetic energy and potential energy of each rigid body are calculated and expressed in the generalized coordinates. Summing over the rigid bodies then gives the total kinetic energy K_s and the total potential energy V_s, yielding

$$L_s(q_s, \dot{q}_s) := K_s(q_s, \dot{q}_s) - V_s(q_s) \tag{1}$$

Lagrange's equation then gives the standard robot equations

$$D_s(q_s)\ddot{q}_s + C_s(q_s, \dot{q}_s)\dot{q}_s + G_s(q_s) = \Gamma_s \tag{2}$$

where the matrix D_s is the mass-inertia matrix, C_s is the matrix of Coriolis and centrifugal terms, G_s is the gravity vector, and Γ_s is the vector of generalized forces acting on the robot. Using the principle of virtual work, Γ_s can be written as

$$\Gamma_s = B_s u + B_{sp}(q_s)\tau_{sp}(q_s, \dot{q}_s) + B_{\text{yaw}}(q_s)\tau_{\text{yaw}}(q_s, \dot{q}_s) \tag{3}$$

where the matrices[1] B_s, B_{sp}, and B_{yaw} define how the motor torques $u = [u_{1R}, u_{2R}, u_{3R}, u_{1L}, u_{2L}, u_{3L}]^T$, the spring torques τ_{sp}, and the stance-leg end yaw torque τ_{yaw} enter the model, respectively. For $i \in \{1R, 2R, 1L, 2L\}$, the spring torque of the i-th series-elastic actuator is modeled as

$$\tau_{sp,i} = -k_{sp,i}(q_i - q_{gr,i}) - b_{sp,i}(\dot{q}_i - \dot{q}_{gr,i}) \tag{4}$$

where $k_{sp,i}$ denotes spring stiffness and $b_{sp,i}$ is a damping coefficient. The primary joint friction is due to the harmonic drives used in the series-elastic actuators and is ignored in the model at the current time. References [32,33] provide nonlinear models of power-loss at the harmonic drives and will be incorporated when sufficient experimental data is available from the robot. The stance-leg end yaw torque is also modeled as viscous friction[2]

$$\tau_{\text{yaw}} = -b_{\text{yaw}}\omega_{\text{shin}}(q_s, \dot{q}_s) \tag{5}$$

where ω_{shin} is the vertical component of the angular velocity about the stance shin and b_{yaw} is a constant.

Setting $x = (q_s; \dot{q}_s) \in TQ_s$, the model in state-variable form is

[1]Because of the way coordinates have been assigned, Bs is a constant matrix. Moreover, because the actuators are independent, Bs has (full) rank equal to the number of actuators, 6.

[2]We anticipate that the assumption of yaw torque in the form of viscous friction will better approximate the behavior of the robot in the laboratory, where a passive foot significantly will reduce yaw, while still allowing the foot to pitch and roll.

$$\dot{x} = \begin{bmatrix} \dot{q}_s \\ D_s^{-1}(q_s)(-H_s(q_s,\dot{q}_s) + B_s u) \end{bmatrix} \tag{6}$$

where

$$H_s(q_s,\dot{q}_s) = C_s(q_s,\dot{q}_s)\dot{q}_s + G_s(q_s) - B_{sp}(q_s)\tau_{sp}(q_s,\dot{q}_s) - B_{\text{yaw}}(q_s)\tau_{\text{yaw}}(q_s,\dot{q}_s) \tag{7}$$

Equation (6) immediately leads to the state variable model

$$\dot{x} = f_s(x) + g_s(x)u \tag{8}$$

4.3 Impact Model. An impact occurs when the end of the swing leg contacts the ground. Let $p_v : Q_s \to \mathbb{R}$ denote the vertical height of the swing leg above the ground so that the impact surface is

$$\mathcal{S} = \{x \in TQ_s \,|\, p_v(q_s) = 0\} \tag{9}$$

The impact is modeled as a contact of two rigid bodies, using the methodology of Ref. [34]; see Ref. [31] for the details. Consequently, the impact is instantaneous; the generalized configuration variables are constant across the impact, while the generalized velocities undergo a jump. The impact map is expressed as

$$x^+ = \Delta(x^-) \tag{10}$$

where x^- is the value of the state just before the impact and x^+ is its value just after the impact.

4.4 Hybrid Model. Combining the single support models and the impact models for the left and right legs results in the hybrid model

$$\Sigma_L : \begin{cases} \dot{x} = f_{s,L}(x) + g_{s,L}(x)u, & x^- \notin \mathcal{S}_L \\ x^+ = \Delta_{L\to R}(x^-), & x^- \in \mathcal{S}_L \end{cases}$$
$$\Sigma_R : \begin{cases} \dot{x} = f_{s,R}(x) + g_{s,R}(x)u, & x^- \notin \mathcal{S}_R \\ x^+ = \Delta_{R\to L}(x^-), & x^- \in \mathcal{S}_R \end{cases} \tag{11}$$

In the hybrid model, the dynamics evolve according to Eq. (8) until the swing leg impacts the ground. The impact map given by Eq. (10) is inactive until the state of the robot reaches the switching surface $\mathcal{S}$, at which point, the impact map becomes active and results in jump (or discontinuity) in the velocity states. Equation (11) gives the hybrid nonlinear system for 3D bipedal walking.

4.5 Planar or 2D Dynamic Model. A sagittal plane model is obtained from the 3D model of Sec. 4.2 by imposing four holonomic constraints and setting the width of the hips to zero. In particular, the yaw and roll coordinates of the torso, q_z and q_y, and their derivatives are set to zero, thereby constraining the torso to the sagittal plane. The hip coordinates q_{3R} and q_{3L} and their derivatives are also set to zero, so that the hip axis is perpendicular to the sagittal plane. The Lagrangian of the planar model is then the Lagrangian of the 3D model restricted to the surface

$$\{(q_s;\dot{q}_s) \in TQ_s \,|\, q_z = 0, q_y = 0, q_{3R} = 0, q_{3L} = 0, \dot{q}_z = 0, \dot{q}_y = 0, \dot{q}_{3R} = 0, \dot{q}_{3L} = 0\} \tag{12}$$

The control torques associated with q_{3R} and q_{3L} are removed, leaving four actuators. The mass of these actuators is retained in the model so that solutions of the 3D and 2D models can be compared.

The impact map is once again developed using the method in Ref. [34]. A hybrid model is then formed, just as in Eq. (11). The model can be simplified to a single-phase system with impulse effects if leg swapping is incorporated into the impact map, as in Ref. [35].

5 Gait Design and Optimization

5.1 General Method. A holonomic constraint that is imposed through the action of an actuator rather than the internal forces of a physical constraint is said to be *virtual* [35–37]. Virtual constraints can be used to synchronize the links of a robot in order to achieve common objectives of walking, such as supporting the torso, advancing the swing leg in relation to the stance leg, specifying foot clearance, etc. Analogous to physical constraints, virtual constraints induce a reduced-dimensional model compatible with the constraints, called the zero dynamics [36,38]. When combined with parameter optimization, virtual constraints can be designed to achieve additional objectives such as walking at a desired speed and respecting bounds on ground reaction forces. Energy efficiency can be increased, as explained in [30,31,36,39]. The main ideas of designing and optimizing periodic walking gaits are summarized below while the details are given in Appendix A. The issue of stability is addressed separately in Sec. 8.

5.2 Virtual Constraints. One virtual constraint per actuator is proposed in the form of an output that, when zeroed by a feedback controller, enforces the constraint. The constraints are written in the form

$$y = h(q_s,\alpha) = h_0(q_s) - h_d(\theta(q_s),\alpha) \tag{13}$$

where $h_0(q_s)$ specifies the vector of variables to be controlled, $h_d(\theta,\alpha)$ is the desired evolution of the controlled variables as a function of $\theta(q_s)$, and $\alpha = [\alpha_{j,i}] \in \mathbb{R}^{6\times(n+1)}$ is a matrix of real parameters to be chosen. The number of columns, $n+1$, is defined later in Sec. 6. A gait-timing variable $\theta(q_s)$ is used to replace time in parameterizing a motion of the robot. Consequently, $\theta(q_s)$ is selected to be strictly monotonic (i.e., strictly increasing or decreasing) along normal walking gaits.

For the 3D model of ATRIAS 2.1 the controlled variables, when the right leg is the stance leg, are initially selected as

$$h_0(q_s) = \begin{bmatrix} \frac{q_{gr1R} + q_{gr2R}}{2} \\ \frac{q_{gr1L} + q_{gr2L}}{2} \\ q_{gr2R} - q_{gr1R} \\ q_{gr2L} - q_{gr1L} \\ q_{3R} \\ q_{3L} \end{bmatrix} = \begin{bmatrix} q_{grR}^{\text{LA}} \\ q_{grL}^{\text{LA}} \\ q_{grR}^{\text{Knee}} \\ q_{grL}^{\text{Knee}} \\ q_R^{\text{Hip}} \\ q_L^{\text{Hip}} \end{bmatrix} \tag{14}$$

where $q_{grR}^{\text{LA}}, q_{grL}^{\text{LA}}, q_{grR}^{\text{Knee}}, q_{grL}^{\text{Knee}}, q_R^{\text{Hip}}$, and q_L^{Hip} are the leg angle for stance leg, leg angle for swing leg, knee angle for stance leg, knee angle for swing leg, hip joint angle for stance leg and hip joint angle for the swing leg, respectively. The first four variables represent quantities in the sagittal plane, on the motor side of the series-compliant actuators; specifically, they correspond to the angles of the right and left legs relative to the torso, and the angles of the knees, respectively, when the springs are at rest. The last two controlled variables are the angles of legs relative to the torso, in the frontal plane; recall that these variables are not actuated through springs.

The gait-timing variable is selected as

$$\theta(q_s) = \begin{cases} \theta_R(q_s) & \text{if the right leg is stance,} \\ \theta_L(q_s) & \text{otherwise} \end{cases} \tag{15}$$

where $\theta_R(q_s)$ is the angle between the virtual leg[3] and the ground surface normal vector when the right leg is the stance leg. $\theta_L(q_s)$ is defined in an analogous manner when the left leg is the stance leg. The desired evolution of the controlled variables, $h_d(\theta(q_s),\alpha)$, will be specified in Sec. 6. The quantity α represents the free coefficients in the family of functions used to design the virtual constraints. The free parameters will be determined based on a finite-dimensional nonlinear optimization problem.

5.3 Zero Dynamics. When the decoupling matrix is invertible, see Refs. [31,36,38], zeroing of the virtual constraints in Eq. (13) via feedback creates a parameterized smooth surface Z_α that is invariant under the flow of the closed-loop single support dynamics. The dynamics restricted to this surface, that is, the dynamics compatible with the constraints, is called the *zero dynamics*. In each single-support phase, the zero dynamics can be expressed in the form of a second-order system

$$D_{\text{zero}}(q_{\text{zero}},\alpha)\ddot{q}_{\text{zero}} + H_{\text{zero}}(q_{\text{zero}},\dot{q}_{\text{zero}},\alpha) = 0 \tag{16}$$

where $(q_{\text{zero}},\dot{q}_{\text{zero}})$ are the unactuated variables in the Lagrangian model and constitute a set of local coordinates for the surface Z_α (see Appendix A for more details). Because the actuators are doing work on the system when zeroing the outputs, the resulting dynamics may not be Lagrangian, although, in special cases, the zero dynamics is Lagrangian [36]. When the virtual constraints in Eq. (13) have vector relative degree two[4] [36,38], as is the case here, the dimension of q_{zero} equals the dimension of q_s minus the number of independent actuators. Hence, for the 3D model used here, $\dim q_{\text{zero}} = 7$ and $q_{\text{zero}} = (q_z; q_y; q_x; q_{1R}; q_{2R}; q_{1L}; q_{2L})$.

5.4 Optimization. As shown in Appendix A, the process of deriving (16) provides a closed-form expression for the control input $u^*_\alpha(q_{\text{zero}},\dot{q}_{\text{zero}})$ achieving

$$0 = h(q_s,\alpha) \Leftrightarrow h_0(q_s) = h_d(\theta,\alpha)$$

that is, the control input that zeros the virtual constraints and creates Z_α. Solutions of the zero dynamics (16) are exact solutions of the full-dimensional model (6) in closed-loop with u^*_α [30,31,40]. This motivates posing an optimization problem to select α resulting in a periodic solution of the hybrid model (11), where the lower-dimensional dynamic equations of the zero dynamics (16) are integrated in place of the full dynamics (8) in closed loop with u^*_α.

The cost function will be taken as the cost of mechanical transport CMT [2]

$$J(\alpha, q^-_{\text{zero}}, \dot{q}^-_{\text{zero}}) = \frac{1}{gM_{\text{tot}}d}\int_0^{T_I}\sum_{i=1}^{6}[p_i(t)]_+ dt \tag{17}$$

where $(q^-_{\text{zero}};\dot{q}^-_{\text{zero}})$ denotes the final condition of the zero dynamics. Furthermore, T_I is the step duration, d represents the distance traveled by the center of mass (COM) in one step, g denotes the gravitational constant, M_{tot} is the total mass of the robot, $p_i(t)$ is actuator power, and $[p]_+ = p$ when $p \geq 0$ and equals zero otherwise. According to Ref. [2], for humans walking at approximately 1 m/s, CMT is approximately 0.05.

The parameter vector α and the final conditions $(q^-_{\text{zero}};\dot{q}^-_{\text{zero}})$ are chosen to minimize $J(\alpha, q^-_{\text{zero}},\dot{q}^-_{\text{zero}})$ subject to the walking gait being periodic and symmetric, the ground reaction forces are feasible, and the speed is a desired value. Here, the minimization was carried out in MATLAB using the fmincon function.

If the optimization process is successful, it returns the (locally) optimized value for the parameters in the virtual constraints, α^* and the final conditions $(q^-_{\text{zero}};\dot{q}^-_{\text{zero}})$ for a periodic solution of the hybrid model (11) corresponding to a walking gait with the specified properties. Section 8 will discuss how the virtual constraints can be used to synthesize a feedback controller that asymptotically stabilizes the walking gait.

6 Parameterization of Desired Trajectories for Holonomic Constraints

6.1 NURB Curves. A NURB curve is defined in a two dimensional homogeneous coordinate space as follows. Let s be related to the gait timing variable by $s = (\theta(q_s) - \theta^+)/(\theta^- - \theta^+)$ and θ^+ and θ^- are the initial and final values of the gait timing variable θ on the periodic orbit, and let $P(s) = (s; h_{d,j}(s)) \in \mathbb{R}^2$ be the 2D position of the points on the NURB curve for the jth output. Then

$$P(s) = \frac{\sum_{i=1}^{n+1} B_i w_i N_{i,k}(s)}{\sum_{i=1}^{n+1} w_i N_{i,k}(s)} = \sum_{i=1}^{n+1} B_i R_{i,k}(s) \tag{18}$$

where $w_i, i = 1,\ldots,n+1$ are nonnegative real scalars, $B_i = (s_i;\alpha_{j,i}) \in \mathbb{R}^2$ is the 2D position of the ith control vertex for the jth output function, $N_{i,k}(s)$ denotes the basis function of order k corresponding to the ith control point defined by *Cox-de Boor* recursion, [41].

$$N_{i,0}(s) = \begin{cases} 1 & s_i \leq s < s_{i+1} \\ 0 & \text{otherwise,} \end{cases} \tag{19}$$

$$N_{i,k}(s) = \frac{(s - s_i)N_{i,k-1}(s)}{s_{i+k-1} - s_i} + \frac{(s_{i+k} - s)N_{i+1,k-1}(s)}{s_{i+k} - s_{i+1}} \tag{20}$$

where s_i are the values of the knot vector $\mathbf{s} = [s_1\ s_2\ \ldots\ s_{n+1}]$ and $s_i < s_{i+1}$, and $n+1$ denotes the number of the control points.

It is worth noting that if the number of the control points and the order of the basis functions are the same, then a NURB curve is equivalent to a Bézier curve [41].

6.2 Advantages of NURBs. Bézier polynomials have been previously used in Refs. [36], [31, Chap. 6], [12], and [30] to parameterize the holonomic constraints for the bipedal robots. As noted above, Bézier polynomials are a special case of NURB curves, and thus using NURBs allows more solutions when designing gaits via optimization, as in Sec. 5.4, which may result in lower values of the cost function.

We offer next a few qualitative reasons for why NURBs yield better results.

6.2.1 Local Action of Control Points. As the order of the NURB basis functions $N_{i,k}(s)$ decreases, the control points affect the curve over smaller ranges of s, which has advantages. For example, Fig. 3 shows $N_{i,k}(s)$, $(\partial N_{i,k}(s)/\partial s)$ and $(\partial^2 N_{i,k}(s)/\partial s^2)$ for $k=6$ (solid line) and $k=3$ (dashed line), with $n=6$. When $k=3$, B_4, B_5, and B_6 have no contribution to the shape of the desired trajectory at $s=0$ because the basis functions $N_{i,k}(s)$ corresponding to those control points vanish at $s=0$. On the other hand, for $k=6$, all of the control points contribute to the value of the trajectory at $s=0$. Figure 3 also shows that when $k=6$, at the boundaries where the control points B_1, B_2, B_5 and B_6 affect $P(s)$, their corresponding basis functions have large values for $(\partial N_{i,k}(s)/\partial s)$ and $(\partial^2 N_{i,k}(s)/\partial s^2)$. This can cause numerical instability of the solutions as a numerical optimizer tries to adjust the control points to minimize cost while achieving periodicity of the solution.

[3]Virtual leg is defined as a virtual line connecting the pivot point of the stance leg to the hip joint.

[4]Essentially means the second derivatives of the six outputs in Eq. (13) depend on six inputs in a full rank or independent manner.

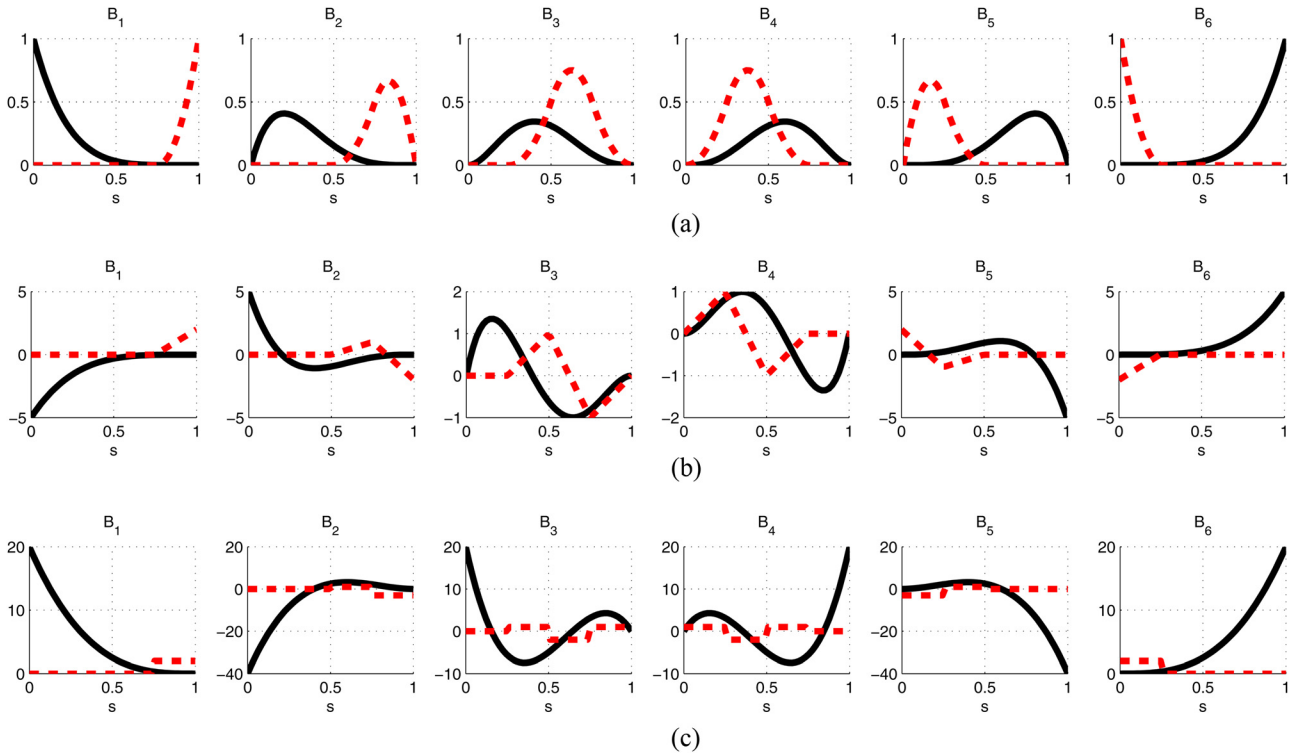

Fig. 3 (*a*) Basis functions, (*b*) first derivative of the basis functions, and (*c*) second derivative of the basis functions, all with respect to the timing variable *s* for each control point B_i when the order *k* is six (solid line) and three (dashed line)

6.2.2 Subphases. Because a Bézier polynomial is an analytic function (in the sense of globally convergent Taylor series), if it (or one of its derivatives) is constant over an open set, then it (or the derivative) is constant everywhere. When $k < n$, a NURB is not an analytic function, and hence, it is possible to have non-trivial regions where the curve or one of its derivative is constant, while the NURB is not globally constant. These regions are informally referred to as "subphases". Figure 4 illustrates this for one of the trajectories associated with the right leg knee angle, in the regions for $s \in [0\ 0.25]$, $s \in [0.25\ 0.5]$, $s \in [0.5\ 0.75]$, and $s \in [0.75\ 1]$. This figure shows that the velocity of the knee angle is commanded to a small value at the beginning of the stance phase. Consequently, the energy of the impact forces F_{impact}, shown in Fig. 5, is directed into the springs, as illustrated by their deflection δ. The energy stored in the springs is released later in the gait.

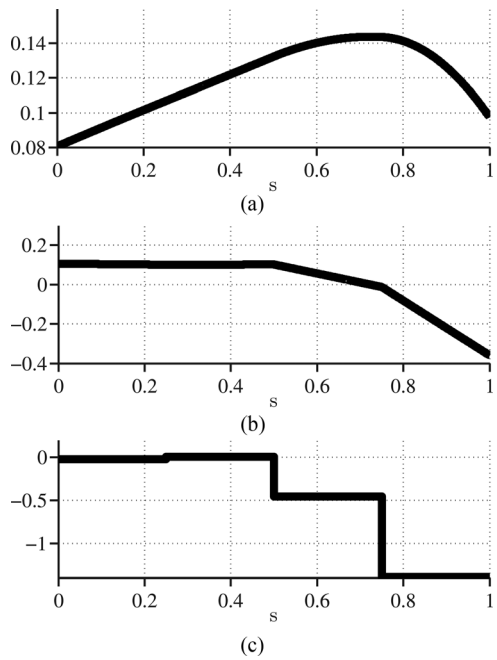

Fig. 4 (*a*) Desired trajectory for right (stance) leg knee angle q^{Knee}_{grR}, (*b*) first derivative of the desired trajectory, and (*c*) the second derivative of the desired trajectory when order of the NURB basis function is 3

7 Performance Analysis of ATRIAS

The optimization framework of Secs. 5 and 6 has been applied to the 3D model of Sec. 4 to compute walking gaits that are locally optimal with respect to CMT. The gaits may only be locally optimal because of the dependence of the cost function (17) on the parameters of the virtual constraints and the final conditions of the zero dynamics is non convex. Simulations for nominal walking speeds of 0.5 to 1.4 (m/s), in increments are 0.1(m/s), are presented. Walking at 1(m/s) is analyzed in greater detail.

7.1 Walking Efficiency Versus Speed. Figure 6 shows the computed CMT versus speed when Bézier and NURB are used as desired trajectories for the holonomic constraints, circles and squares respectively. For comparison purposes, the CMT of a human is estimated from experimental data to be 0.05 at a speed of 1(m/s) [2], while the experimentally estimated CMT of the Cornell Biped is 0.04 at a speed of 0.6(m/s) [42]. Interpolating a cubic polynomial through the NURB-based simulation data of ATRIAS 2.1 results in a minimum CMT of 0.05 at 0.7(m/s). At 1(m/s), the simulated CMT of ATRIAS is 0.096, which means the robot would require approximately twice the power of a human when walking at 1(m/s), assuming once again that the harmonic drives are lossless.

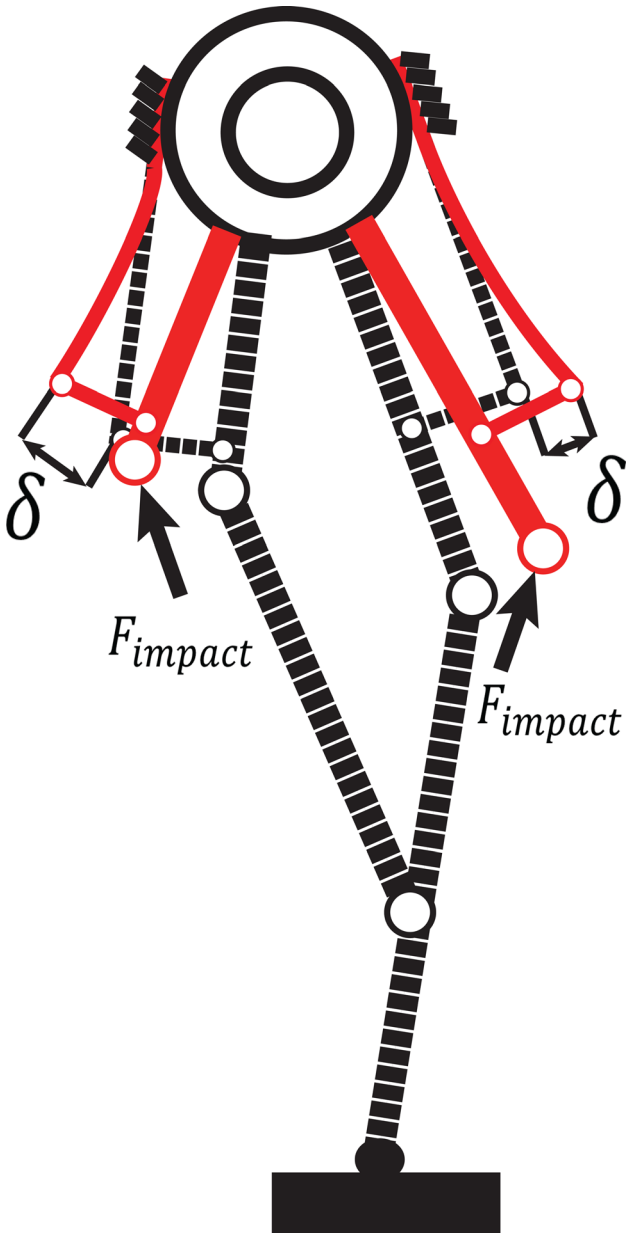

Fig. 5 Leg shortly after impact, showing the springs absorbing the impact energy

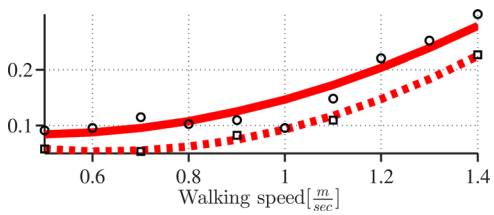

Fig. 6 Circles represent computed CMT using Bézier curves for the desired trajectories versus walking speed from 0.5 to 1.4(m/s). The thick solid line is a cubic interpolation of these data. Squares represent computed CMT using NURB curves versus walking speeds 0.5, 0.7, 0.9, 1.1, and 1.4(m/s). The dashed line is a cubic interpolation of these data. Losses at the harmonic drives are ignored

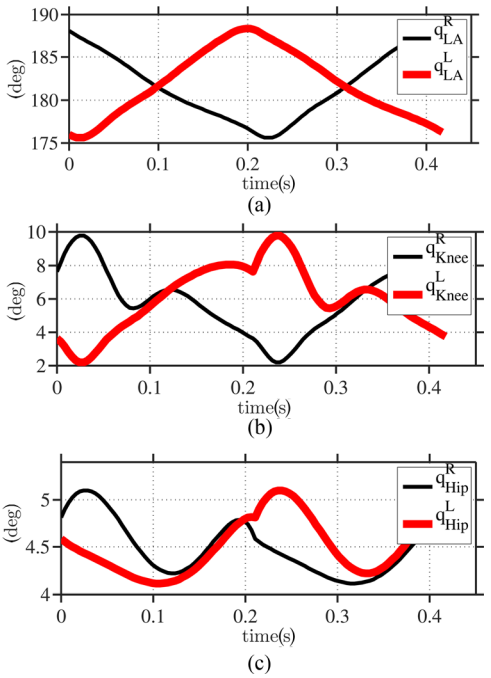

Fig. 7 Evolution during one step of (*a*) the right leg angle q^R_{LA} and the left leg angle q^L_{LA}, (b) the right knee angle q^R_{Knee} and the left knee angle q^L_{Knee}, (*c*) the right hip joint angle q^R_{Hip} and the left hip joint angle q^L_{Hip} for an optimal walking motion with the nominal velocity of 1.0(m/s) and CMT 0.096

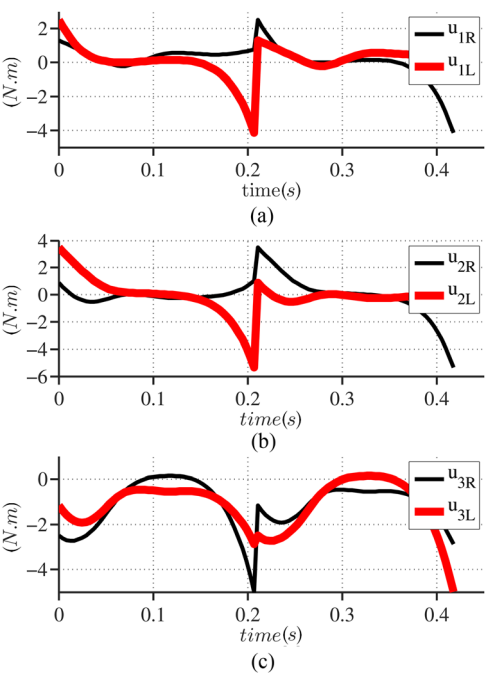

Fig. 8 Control effort during one step for (*a*) u_{1R}, u_{1L}, (*b*) u_{2R}, u_{2L}, and (*c*) u_{3R}, u_{3L} corresponding to a fix point with nominal walking speed of 1.0(m/s) and CMT 0.096

If the harmonic drives are assumed to be 70% efficient on average, then the motors in the sagittal plane must produce approximately 43% more power when realizing the walking gaits of Fig. 6. When this is taken into account, ATRIAS's estimated CMT at 0.7(m/s) is 0.071, or approximately one and a half times that of a human, while at 1(m/s), CMT would 0.13, or approximately two and a half times that of a human.

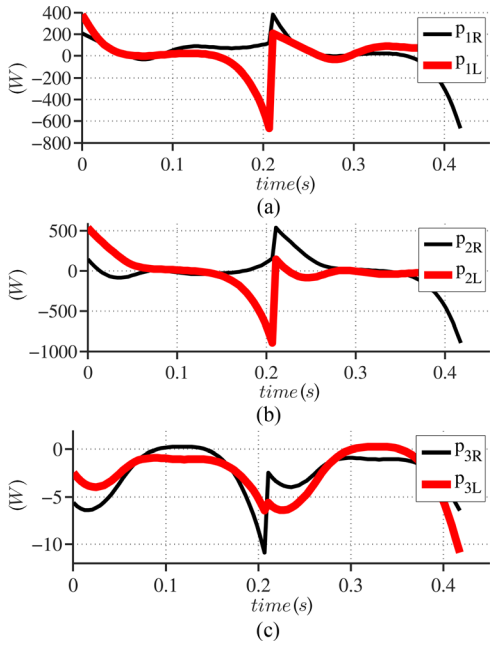

Fig. 9 Actuation power during one step for (*a*) p_{1R}, p_{1L}, (*b*) p_{2R}, p_{2L}, and (*c*) p_{3R}, p_{3L} corresponding to a fix point with nominal walking speed of 1.0(m/s) and CMT 0.096

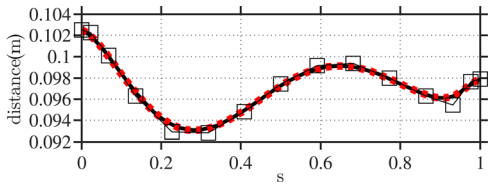

Fig. 10 NURB curve of order 5 with 15 control point is fitted to the trajectory of the horizontal distance between the end of the left leg and the COM in the frontal plane, solid curve is the distance trajectory, dashed curve is the fitted data and the squares are the control points of the NURB curve.

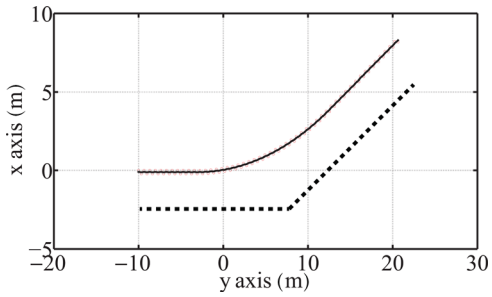

Fig. 11 Top curve is the (*x* – *y*)-plane projection of the center of mass and foot positions to achieve steering along a desired path with a 30 deg deflection with respect to the *y*-axis. The lower curve is the commanded path, shifted by 2.5 m. Convergence to the desired path is clear.

7.2 Walking at 1 (m/s). A periodic walking gait optimized at 1(m/s) is analyzed in more detail. In the following, the right l6eg is the stance leg while the left leg is the swing leg.

The evolution of the virtual constraints is shown in Fig. 7. The motor-side right leg angle q_{grR}^{LA} decreases from 187 deg to 175 deg and the corresponding left leg angle q_{grL}^{LA} increases from 175 deg to 187 deg. The motor-side right knee angle q_{grR}^{Knee} varies between 4 deg and 10 deg and the left knee angle q_{grL}^{Knee} varies from 2 deg to 8 deg. In the frontal plane, the right hip joint angle q_{Hip}^{R} and the left hip joint angle q_{Hip}^{L} shown in Fig. 7(*c*) are essentially constant, being bounded between 4 deg and 5 deg.

Figure 8 shows the motor torques for u_{1R}, u_{1L}, u_{2R}, u_{2L}, u_{3R}, and u_{3L}, while Fig. 9 shows the corresponding actuator power (product of torque and angular velocity at the motor shafts). Table 1 presents the amount of the positive work performed by each actuators as well as the amount of the negative work absorbed by each actuators over the course of a single step. A notable point is the large amount of negative work done by actuator u_1 of the stance leg. Due to the 4-bar linkage, u_1 is positive to support the robot but moves in the negative direction to advance the body of the robot.

8 Feedback Stabilization

8.1 Input–Output Linearization. Each of the gaits presented in Sec. 7 comes with a set of outputs (i.e., virtual constraints) which vanish on the periodic orbit traced out by the robot's states over the periodic walking motion. Let α^* denote the vector of the free parameters resulting from the optimization of the virtual constraints, giving

$$y = h(q_s, \alpha^*) = h_0(q_s) - h_d(\theta(q_s), \alpha^*) \tag{21}$$

A feedback controller is required to impose the constraints by driving the outputs to zero when the robot is away from the periodic orbit. A Poincaré analysis is then done to assess the stability of the closed-loop system.

Our first step in the design of the feedback controller is optional: we augment the virtual constraints given in Eq. (21) with a term $h_c(q_s)$ that vanishes on the periodic orbit and hence leaves the walking motion unchanged [40] and [30], Eq. (21). The extra term has the effect of smoothing the torques at leg transition and creating hybrid invariance. The augmented output is then

$$y = \tilde{h}(q_s) = h_0(q_s) - h_d(\theta(q_s), \alpha^*) - h_c(q_s) \tag{22}$$

Assuming the decoupling matrix $A(x)$ is invertible (see Eq. (B5) of Appendix B), input-output linearization yields the feedback controller

$$u(x) = u^*(x) - A(x)^{-1}\left(\frac{1}{\varepsilon^2}K_P y + \frac{1}{\varepsilon}K_D \dot{y}\right) \tag{23}$$

which renders the input-output map linear, namely

Table 1 The energy breakdown over one step for walking at 1.0(m/s); right leg is stance. The CMT is 0.096

Actuator	Positive work (Joule)	Negative work (Joule)	Peak power (W)	Peak torque (N m)
u_{1R}	0.154	3.605	84.518	4.154
u_{2R}	1.711	1.265	113.720	5.358
u_{3R}	0.429	0.608	42.834	4.989
u_{1L}	1.339	1.487	174.23	4.154
u_{2L}	4.434	3.444	391.780	5.358
u_{3L}	0.283	0.330	27.298	4.989

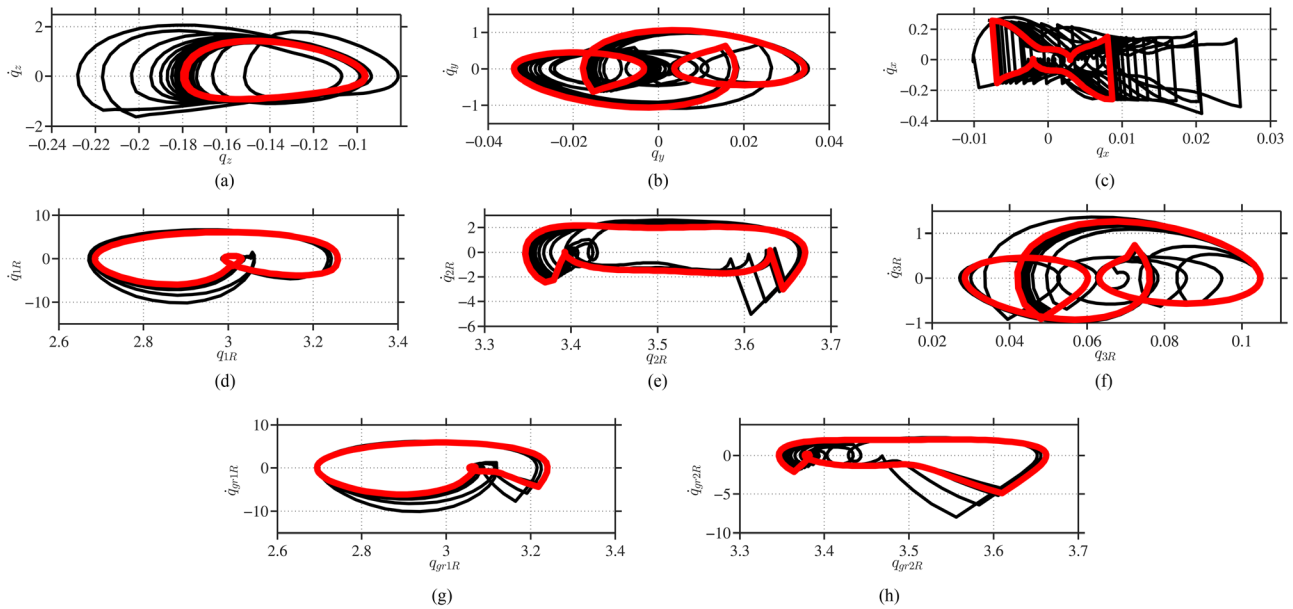

Fig. 12 Convergence of the trajectories to the fixed point after perturbing the initial condition

$$\ddot{y} + \frac{1}{\varepsilon} K_D \dot{y} + \frac{1}{\varepsilon^2} K_p y = 0 \tag{24}$$

The control gains K_P and K_D are chosen such that the matrix

$$\begin{bmatrix} 0 & I \\ -K_D & -K_P \end{bmatrix}$$

is Hurwitz and $\varepsilon > 0$ is a tuning parameter.

The feedback controller in Eq. (23) was implemented on the 3D model for the nominal walking speed of 1.0(m/s). The stability of the fixed point is checked using a linearized Poincaré map $P : \Delta\mathcal{S} \to \Delta\mathcal{S}$, where $x_{j+1} = P(x_j)$ and $\Delta\mathcal{S}$ is the Poincaré section taken at the map of the switching surface by the impact. $x_j = (q_z; q_y; \ldots; \dot{q}_z; \dot{q}_y; \ldots) \in \Delta\mathcal{S}$ denotes the projection of the state vector for the full dynamics model during step j onto $\Delta\mathcal{S}$. Because the Poincaré section $\Delta\mathcal{S}$ is a hyperspace in $\mathbb{R}^{26}$, the Poincaré section has twenty five independent components. To implement this, define a projection map $\Pi(x) = (q_z; q_y; \ldots; \dot{q}_z; \dot{q}_y; \ldots)$ which eliminates q_x (pitch angle) from the state vector and also defining perturbations as $\delta x_j = \Pi(x_j - x^*)$, the linearization of the Poincaré map around the fixed point x^* results in the Jacobian $A = \partial P / \partial x$ of the Poincaré map. In particular

$$A_j = \frac{P(x^* + \Delta x_j) - P(x^* - \Delta x_j)}{2\Delta x_j} \tag{25}$$

where A_j is jth column of $A = [A_1, A_2, \ldots, A_{25}]$ and $\Delta x_j = (0; \ldots; 0; \varepsilon_j; 0; \ldots; 0)$. Using the output functions explained in (14) and computing the linearized Poincaré map for $\varepsilon = 0.01$. The feedback controller of Eq. (23) makes the zero dynamics manifold hybrid invariant and attractive. As expected from Ref. [30], calculations show that one eigenvalue has magnitude greater than one and hence the gait is unstable under this controller.

8.2 Event-Based Stabilization. On the other hand, when the virtual constraints are applied to the 2D model of Sec. 4.5 (with the virtual constraints for q_{3R} and q_{3L} removed from the controller), a stable gait is achieved. Based on this fact, one suspects that the instability of the 3D model is due to the roll or yaw motions. From [30], the position of the COM in the frontal plane is important. If at leg touchdown, the COM is not between the feet, but outside the position of the next supporting foot, the robot will topple sideways. Based on this physical intuition, the control of the variable q_3 (which regulates step width on the swing leg) was replaced by the control of the distance between the swing leg end and the COM along the frontal direction. The distance between the end of the swing leg and the COM of the robot in the frontal plane is computed.[5] Then, a NURB curve, see Fig. 10, of order five with fifteen control points is fit to this distance. Next, an event based controller is designed and integrated with the continuous input output linearizing controller in Eq. (23). To achieve this goal, as in [30], Eq. (26) we augment the output with a term h_s parameterized by a vector β, which is held constant over two steps and is updated at the left-to-right impact event. In particular, the augmented output function is written as

$$y = \tilde{h}(q_s) = h_0(q_s) - h_d(\theta(q_s), \alpha^*) - h_c(q_s) - h_s(q_s, \beta) \tag{26}$$

Finally, the Poincaré map $x_{j+1} = P(x_j, \beta_j)$ is linearized around the fixed point x^* and β^* as $\delta x_{j+1} = (\partial P(x, \beta)/\partial x)\delta x_j + (\partial P(x, \beta)/\partial \beta)\delta \beta_j$, where $\delta \beta_j = \beta_j - \beta^*$. A state feedback law $\delta \beta_j = -K \delta x_j$ is designed such that $A - BK$ is Hurwitz. K is found through discrete LQR algorithm and the two largest eigenvalues in magnitude for the closed loop system are $|\lambda_1| = 0.74$ and $|\lambda_2| = 0.066$, proving stability. Figure 12 shows the convergence of the phase portrait for $(q_x, \dot{q}_x), (q_y, \dot{q}_y), (q_z, \dot{q}_z)$, $(q_{1R}, \dot{q}_{1R})$, $(q_{2R}, \dot{q}_{2R}), (q_{3R}, \dot{q}_{3R})$, $(q_{gr1R}, \dot{q}_{gr1R})$, and $(q_{gr2R}, \dot{q}_{gr2R})$ after perturbing the fixed point.

8.3 Steering Via Event-Based Control. In this section, the stabilizing two-step event-based controller is modified according to Ref. [43] to achieve slow steering along a desired direction. Due to the yaw-invariance property of the designed output functions, the input-output linearizing feedback law is yaw invariant and hence, the resultant hybrid model of walking without the event-based portion is equivariant under yaw rotations. This means that if the robot is initialized from a given pose and

[5] Frontal plane is attached to the torso and the normal axis is aligned with y axis of the torso frame.

advances t units of time and then its state is rotated by g radians about the z-axis, this would be equivalent to the case that initial pose is first rotated by g radians about the z-axis and then the robot walks for t units of time. Next, the exponential stability of the fixed point results in local input-to-state stability (ISS) of the discrete-time control system defined by the Poincaré map. Thus, all assumptions of Proposition 6 of Ref. [43] are satisfied and we can modify the parameters in the virtual constraints to affect the relative step lengths of the right and left legs, and thereby steer the robot. Figure 11 depicts the top view of the COM and foot placement trajectories to achieve steering along a desired path with a 30 deg angle with respect to the horizontal line (y-axis).

9 Conclusions

The 3D bipedal robot ATRIAS 2.1 has 6 actuators, and when in single support, it has 13 DOF. To the best of the authors' knowledge, no bipedal robot has been successfully controlled with this much underactuation. The paper showed that the method of virtual constraints and hybrid zero dynamics could be used to design energetically efficient gaits with respect to the CMT and to stabilize them. For the process of gait optimization, nonuniform rational basis spline (NURB) were used to parameterize the virtual constraints; these functions provided more flexibility than the Bézier curves that have previously been used for this purpose.

Stable walking of the robot attached to a boom has been demonstrated; a video is available online [3]. The gait was designed using the virtual constraints of the 1 m/s gait presented herein, with the lateral virtual constraints replaced by constant set points. Currently, the 3D model is being refined and experiments in 3D are being planned. In addition, the electronics of the robot are being refined so that energy consumption can be measured and logged in real time.

Acknowledgment

This work was supported by DARPA Contract W91CRB-11-1-0002. Ching-Long Shih and Christine Chevallereau made valuable contributions to the Lagrangian model of ATRIAS 2.1.

Appendix A: Single-Support Zero Dynamics

This section presents a derivation of the zero dynamics of ATRIAS 2.1 in single support. Suppose that θ is given by

$$\theta(q_s) = c_0 q_s + c_1 \tag{A1}$$

for an appropriate row vector c_0 and scalar c_1. Let $q_{\text{cont}} = h_0(q_s)$ denote the controlled variables in the output in Eq. (13) and suppose that q_{cont} can be expressed as an affine function of the configuration variables.

$$q_{\text{cont}} = \tilde{H}_0 q_s + \tilde{H}_1 \tag{A2}$$

Let q_{zero} be a complementary set of variables satisfying

$$q_{\text{zero}} = \hat{H}_0 q_s + \hat{H}_1 \tag{A3}$$

and selected so that

$$\bar{q} = \begin{bmatrix} q_{\text{cont}} \\ q_{\text{zero}} \end{bmatrix} \tag{A4}$$

is a set of generalized coordinates for Q_s. Define

$$H_0 = \begin{bmatrix} \tilde{H}_0 \\ \hat{H}_0 \end{bmatrix}, \quad H_1 = \begin{bmatrix} \tilde{H}_1 \\ \hat{H}_1 \end{bmatrix}$$

where it follows that H_0 has (full) rank equal to the dimension of Q_s. Defining

$$T_0 = H_0^{-1} \quad \text{and} \quad T_1 = -H_0^{-1} H_1$$

leads to

$$q_s = T_0 \bar{q} + T_1 \tag{A5}$$

ASSUMPTIONS:

(1) The controlled variables q_{cont} in Eq. (A2), the gait-timing variable $\theta(q_s)$ in Eq. (A1), and the desired evolution $h_d(\theta)$ in Eq. (13) have been selected so that the decoupling matrix (B5) is invertible.

(2) The complementary variables q_{zero} of Eq. (A3) have been selected so that

$$T_0' B = \begin{bmatrix} \bar{B}_1 \\ 0 \end{bmatrix}$$

and $\bar{B}_1$ is 6×6, that is, it is square with size determined by the number of actuators.

(3) The gait-timing variable can be expressed in terms of q_{zero}, that is

$$\theta(\bar{q}) = \bar{c}_0 q_{\text{zero}} + \bar{c}_1 \tag{A6}$$

Expressing the mechanical model (2) in the coordinates (A4) leads to

$$\bar{D}(\bar{q})\ddot{\bar{q}} + \bar{H}(\bar{q}, \dot{\bar{q}}) = \bar{B} u \tag{A7}$$

where

$$\bar{D}(\bar{q}) = T_0' D_s(q_s) T_0 \big|_{q_s = T_0 \bar{q} + T_1} \tag{A8}$$

$$\bar{H}(\bar{q}, \dot{\bar{q}}) = T_0' H_s(q_s, \dot{q}_s) T_0 \Big|_{\substack{q_s = T_0 \bar{q} + T_1 \\ \dot{q}_s = T_0 \dot{\bar{q}}}} \tag{A9}$$

and

$$\bar{B} = T_0' B_s \tag{A10}$$

In the transformed coordinates, the dynamic model can be partitioned as

$$\begin{bmatrix} \bar{D}_{11}(\bar{q}) & \bar{D}_{12}(\bar{q}) \\ \bar{D}_{21}(\bar{q}) & \bar{D}_{22}(\bar{q}) \end{bmatrix} \begin{bmatrix} \ddot{q}_{\text{cont}} \\ \ddot{q}_{\text{zero}} \end{bmatrix} + \begin{bmatrix} \bar{H}_1(\bar{q}, \dot{\bar{q}}) \\ \bar{H}_2(\bar{q}, \dot{\bar{q}}) \end{bmatrix} = \begin{bmatrix} \bar{B}_1 \\ 0 \end{bmatrix} u \tag{A11}$$

The zero dynamic is the unactuated part of this model, namely

$$\bar{D}_{21}(\bar{q})\ddot{q}_{\text{cont}} + \bar{D}_{22}(\bar{q})\ddot{q}_{\text{zero}} + \bar{H}_2(\bar{q}, \dot{\bar{q}}) = 0 \tag{A12}$$

We now bring the virtual constraints into consideration

$$0 = q_{\text{cont}} - h_d(\theta) \tag{A13}$$

that is,

$$q_{\text{cont}} = h_d(\theta) \tag{A14}$$

Computing the derivatives of q_{cont} with respect to time so that we can substitute into Eq. (A12) gives

$$\dot{q}_{\text{cont}} = \frac{\partial h_d(\theta)}{\partial \theta} \dot{\theta} \tag{A15}$$

and

$$\ddot{q}_{\text{cont}} = \frac{\partial h_d(\theta)}{\partial \theta}\ddot{\theta} + \frac{\partial^2 h_d(\theta)}{\partial \theta^2}(\dot{\theta})^2 \tag{A16}$$

Equation (A6) yields

$$\dot{\theta} = \bar{c}_0 \dot{q}_{\text{zero}} \tag{A17}$$

$$\ddot{\theta} = \bar{c}_0 \ddot{q}_{\text{zero}} \tag{A18}$$

Substituting these expressions into (A12) and simplifying leads to[6]

$$D_{\text{zero}}(q_{\text{zero}})\ddot{q}_{\text{zero}} + H_{\text{zero}}(q_{\text{zero}}, \dot{q}_{\text{zero}}) = 0 \tag{A19}$$

where

$$D_{\text{zero}} = \bar{D}_{22} + \bar{D}_{21}\frac{\partial h_d(\theta)}{\partial \theta}\bar{c}_0 \tag{A20}$$

and

$$H_{\text{zero}} = \bar{H}_1 + \bar{D}_{21}\frac{\partial^2 h_d(\theta)}{\partial \theta^2}(\dot{\theta})^2 \tag{A21}$$

The control signal u compatible with the virtual constraints being zeroed can also be computed from Eqs. (A11), (A16), and (A18)

$$u^* = \bar{B}_1^{-1}\left\{\left[\bar{D}_{12} + \bar{D}_{11}\frac{\partial h_d(\theta)}{\partial \theta}\bar{c}_0\right]\ddot{q}_{\text{zero}} + \bar{H}_1 + \bar{D}_{11}\frac{\partial^2 h_d(\theta)}{\partial \theta^2}(\dot{\theta})^2\right\} \tag{A22}$$

Appendix B: Feedback Control Details

Consider the following output function representing a virtual constraint as in Eq. (22)

$$y = \tilde{h}(q_s) \tag{B1}$$

The first derivative of y along the solutions of the single-support phase model (2) is simply

$$\dot{y} = \frac{\partial \tilde{h}(q_s)}{\partial q_s}\dot{q}_s \tag{B2}$$

and the second derivative is

$$\ddot{y} = -\frac{\partial \tilde{h}(q_s)}{\partial q_s}D_s^{-1}(q_s)H_s(\dot{q}_s, q_s) \tag{B3}$$

$$+\frac{\partial}{\partial q_s}\left(\frac{\partial \tilde{h}(q_s)}{\partial q_s}\dot{q}_s\right)\dot{q}_s + \frac{\partial \tilde{h}(q_s)}{\partial q_s}D_s^{-1}(q_s)B_s u \tag{B4}$$

The decoupling matrix is given by

$$A(q_s, \dot{q}_s) = \frac{\partial \tilde{h}(q_s)}{\partial q_s}D_s^{-1}(q_s)B_s \tag{B5}$$

while u^* is obtained by solving for the input that sets $\ddot{y} = 0$, giving

$$u^*(q_s, \dot{q}_s) = A^{-1}(q_s, \dot{q}_s)\left(\frac{\partial}{\partial q_s}\left(\frac{\partial \tilde{h}(q_s)}{\partial q_s}\dot{q}_s\right)\dot{q}_s - \frac{\partial \tilde{h}(q_s)}{\partial q_s}D_s^{-1}(q_s)H_s(\dot{q}_s, q_s)\right) \tag{B6}$$

[6]When the decoupling matrix is invertible, D_{zero} is guaranteed to be invertible as well.

References

[1] Grimes, J. A., and Hurst, J. W., 2012, "The Design of ATRIAS 1.0 a Unique Monoped, Hopping Robot," Proceedings of the 2012 International Conference on Climbing and Walking Robots and the Support Technologies for Mobile Machines, pp. 548–554.

[2] Collins, S. H., Ruina, A., Tedrake, R., and Wisse, M., 2005, "Efficient Bipedal Robots Based on Passive-Dynamic Walkers," Science, **307**, pp. 1082–1085.

[3] Grizzle, J., 2012, "ATRIAS 2.1 First Steps," http://www.youtube.com/watch?v=uVkQ5ytOg54&list=UUMfDV8rkQqWhUwnTAYAq0tQ&index=2&feature=plpp_video

[4] Blickhan, R., 1989, "The Spring Mass Model for Running and Hopping," J. Biomech., **22**(11–12), pp. 1217–1227.

[5] McMahon, T. A., and Cheng, G. C., 1990, "The Mechanics of Running: How Does Stiffness Couple With Speed?," J. Biomech., **23**, pp. 65–78.

[6] Farley, C. T., Glasheen, J., and McMahon, T. A., 1993, "Running Springs: Speed and Animal Size," J. Exp. Biol., **185**,, pp. 71–86.

[7] Full, R. J., and Farley, C. T., 2000, "Musculoskeletal Dynamics in Rhythmic Systems—A Comparative Approach to Legged Locomotion," *Biomechanics and Neural Control of Posture and Movement*, J. M. Winters and P. E. Crago, eds. Springer-Verlag, New York.

[8] Seyfarth, A., Geyer, H., Gunther, M., and Blickhan, R., 2001, "A Movement Criterion for Running," J. Biomech., **35**, pp. 649–655.

[9] Raibert, M., 1986, *Legged Robots that Balance*, MIT Press, Cambridge, MA.

[10] Zeglin, G., and Brown, H. B., 1998, "Control of a Bow Leg Hopping Robot," IEEE International Conference on Robotics and Automation.

[11] Ahmadi, M., and Buehler, M., 2006, "Controlled Passive Dynamic Running Experiment With the ARL Monopod II," IEEE Trans. Robotics, **22**, pp. 974–986.

[12] Sreenath, K., Park, H.-W., Poulakakis, I., and Grizzle, J. W., 2011, "Compliant Hybrid Zero Dynamics Controller for Achieving Stable, Efficient and Fast Bipedal Walking on MABEL," Int. J. Robot. Res., **30**(9), pp. 1170–1193.

[13] Sreenath, K., Park, H.-W., and Grizzle, J., 2012, "Design and Experimental Implementation of a Compliant Hybrid Zero Dynamics Controller With Active Force Control for Running on MABEL," International Conference on Robotics and Automation (ICRA), pp. 51–56.

[14] Park, H.-W., Sreenath, K., Ramezani, A., and Grizzle, J., 2012, "Switching Control Design for Accommodating Large Step-Down Disturbances in Bipedal Robot Walking," International Conference on Robotics and Automation (ICRA), pp. 3331–3450.

[15] Park, H.-W., Ramezani, A., and Grizzle, J., 2013, "A Finite-State Machine for Accommodating Unexpected Large Ground-Height Variations in Bipedal Robot Walking," IEEE Trans. Rob. Autom., **29**, pp. 45–50.

[16] Geyer, H., Seyfarth, A., and Blickhan, R., 2006, "Compliant Leg Behaviour Explains the Basic Dynamics of Walking and Running," Proc. R. Soc., London, Ser. B, **273**, pp. 2861–2867.

[17] Laboratory, D. R., 2012, "SolidWorks—Model Parameters for ATRIAS Based on Solidworks," http://code.google.com/p/atrias/

[18] Hodgins, J. K., and Raibert, M. H., 1991, "Adjusting Step Length for Rough Terrain Locomotion," IEEE Trans. Rob. Autom., **7**(3), pp. 289–298.

[19] Ahmadi, M., and Buehler, M., 1999, "The ARL Monopod II Running Robot: Control and Energetics," IEEE International Conference on Robotics and Automation, pp. 1689–1694.

[20] Chevallereau, C., Abba, G., Aoustin, Y., Plestan, F., Westervelt, E. R., Canudas-de-Wit, C., and Grizzle, J. W., 2003, "RABBIT: A Testbed for Advanced Control Theory," IEEE Control Syst. Mag., **23**(5), pp. 57–79.

[21] Corp., H., "Asimo Humanoid Robot," http://world.honda.com/asimo/

[22] McGeer, T., 1988, "Stability and Control of Two-Dimensional Biped Walking," Center for Systems Science, Simon Fraser University, Burnaby, B.C., Canada, Technical Report 1.

[23] McGeer, T., 1990, "Passive Dynamic Walking," Int. J. Robot. Res., **9**(2), pp. 62–82.

[24] Collins, S. H., Wisse, M., and Ruina, A., 2001, "A 3-D Passive Dynamic Walking Robot With Two Legs and Knees," Int. J. Robot. Res., **20**, pp. 607–615.

[25] Pratt, J., and Pratt, G., 1998, "Exploiting Natural Dynamics in the Control of a Planar Bipedal Walking Robot," Proceedings of the Thirty-Sixth Annual Allerton Conference on Communication, Control, and Computing.

[26] Playter, R., Buehler, M., and Raibert, M., 2006, "Bigdog," Proceedings of SPIE International Society for Optical Engineering, G. R. Gerhart, C. M. Shoemaker, and D. W. Gage, eds., SPIE, Vol. 6230.

[27] Robinson, D. W., Pratt, J. E., Paluska, D. J., and Pratt, G. A., 1999, "Series Elastic Actuator Development for a Biomimetic Walking Robot," IEEE/ASME International Conference on Advanced Intelligent Mechatronics, pp. 561–568.

[28] Boaventura, T., Semini, C., Buchli, J., Frigerio, M., Focchi, M., and Caldwell, D. G., 2012, "Dynamic Torque Control of a Hydraulic Quadruped Robot," IEEE Conference on Robotics and Automation, pp. 1189–1894.

[29] Kim, S., 2012, "Biomimetics Robotics Lab," http://sangbae.scripts.mit.edu/biomimetics/videos/

[30] Chevallereau, C., Grizzle, J., and Shih, C., 2009, "Asymptotically Stable Walking of a Five-Link Underactuated 3D Bipedal Robot," IEEE Trans. Rob. Autom., **25**(1), pp. 37–50.

[31] Westervelt, E. R., Grizzle, J. W., Chevallereau, C., Choi, J., and Morris, B., 2007, *Feedback Control of Dynamic Bipedal Robot Locomotion. Control and Automation*, CRC Press, Boca Raton, FL.

[32] Tuttle, T., and Seering, W., 1996, "A Nonlinear Model of a Harmonic Drive Gear Transmission," IEEE Trans. Rob. Autom., **12**(3), pp. 368–374.

[33] Kennedy, C., and Desai, J., 2005, "Modeling and Control of the Mitsubishi pa-10 Robot Arm Harmonic Drive System," IEEE/ASME Trans. Mechatron., **10**(3), pp. 263–274.
[34] Hurmuzlu, Y., and Chang, T., 1992, "Rigid Body Collisions of a Special Class of Planar Kinematic Chains," IEEE Trans. Syst. Man Cybern., **22**(5), pp. 964–971.
[35] Grizzle, J. W., Abba, G., and Plestan, F., 2001, "Asymptotically Stable Walking for Biped Robots: Analysis Via Systems With Impulse Effects," IEEE Trans. Autom. Control, **46**, pp. 51–64.
[36] Westervelt, E., Grizzle, J., and Koditschek, D., 2003, "Hybrid Zero Dynamics of Planar Biped Walkers," IEEE Trans. Autom. Control, **48**(1), pp. 42–56.
[37] Canudas-de-Wit, C., 2004, "On the Concept of Virtual Constraints as a Tool for Walking Robot Control and Balancing," Annu. Rev. Control, **28**, pp. 157–166.
[38] Isidori, A., 1995, *Nonlinear Control Systems: An Introduction*, 3rd ed., Springer-Verlag, Berlin, Germany.
[39] Sreenath, K., Park, H., Poulakakis, I., and Grizzle, J., 2011, "A Compliant Hybrid Zero Dynamics Controller for Stable, Efficient, and Fast Bipedal Walking on MABEL," Int. J. Robot. Res., **30**, pp. 1170–1193.
[40] Morris, B., and Grizzle, J. W., 2009, "Hybrid Invariant Manifolds in Systems With Impulse Effects With Application to Periodic Locomotion in Bipedal Robots," IEEE Trans. Autom. Control, **54**(8), pp. 1751–1764.
[41] Piegl, L., and Tiller, W., 1997, *The NURBS Book*, Springer, New York.
[42] Ruina, A., 2012, "Cornell Ranger, 2011 4-Legged Bipedal Robot," Nov. http://ruina.tam.cornell.edu/research/topics/locomotion_and_robotics/ranger/Ranger2011/index.html
[43] Shih, C., Grizzle, J., and Chevallereau, C., 2012, "From Stable Walking to Steering of a 3D Bipedal Robot With Passive Point Feet," Robotica, **30**, pp. 1119–1130.